J|A|C|S ARTICLES

Published on Web 04/20/2010

Scaling Dopant States in a Semiconducting Nanostructure by Chemically Resolved Electron Energy-Loss Spectroscopy: A Case Study on Co-Doped ZnO

Xuefeng Wang,*,†,‡ Fengqi Song,*,§ Qian Chen,|| Tingyu Wang,† Jinlan Wang,|| Peng Liu,‡ Mingrong Shen,‡ Jianguo Wan,§ Guanghou Wang,§ and Jian-Bin Xu⊥

Australian Key Centre for Microscopy and Microanalysis, The University of Sydney, NSW 2006, Australia, Department of Physics, Soochow University, Suzhou 215006, People's Republic of China, National Laboratory of Solid State Microstructures and Department of Physics, Nanjing University, Nanjing 210093, People's Republic of China, Department of Physics, Southeast University, Nanjing 211189, People's Republic of China, and Department of Electronic Engineering, The Chinese University of Hong Kong, Shatin, New Territories, Hong Kong, People's Republic of China

Received February 5, 2010; E-mail: xfwang1980@gmail.com; songfengqi@nju.edu.cn

Abstract: Dilute dopant introduces foreign states to the electronic structures of host semiconductors and imparts intriguing properties to the materials. Identifying and positioning the dopant states are of crucial importance for seeking the underlying mechanism in the doped systems. However, such determination has still been challenging, particularly for individual nanostructured materials, due to the lack of the spectroscopic probe that possesses both nanometer spatial resolution and chemical resolution. Here, we shall demonstrate the successful scaling of dopant states of individual semiconducting nanostructures by chemically resolved electron energy-loss spectroscopy (EELS), taking the individual Co-doped ZnO nanorods as an example. Guided by the Co dopant spatial distribution mapped by the core-loss EELS technique, chemical resolution is achieved in the accumulated valence electron energy-loss spectra. Three Co dopant states are successfully identified and positioned in the host ZnO bands. Furthermore, the electron extension degrees of the Co dopant states are assessed on the basis of the multiple-atom effect. The above experimental inputs optimize the density functional theoretical calculations, which generates the corrected full electronic structures of (Zn,Co)O dilute magnetic semiconductors. These results give a carrier-mediated interpretation for the room-temperature ferromagnetism of Co-doped ZnO nanostructures based on a recent theory.

I. Introduction

Doping can impart extra functionalities into host semiconductors doped with intentional impurities, allowing for diverse device applications.[1−5] In the molecular-orbital picture, dopant ions introduce atom-like foreign energy levels,[6] which undergo changes in degeneracy and spin states upon the application of crystal field. In order to understand that how the dilute dopant ions drive the functionality of the whole body, one should know how discrete energy levels incorporate into the host energy bands. This is the critical point in the current dilute magnetic semiconductors (DMSs) that have attracted global interest due to their promising applications in future spintronic devices.[7] The origin of magnetism in DMSs has been very controversial.[8] Even nonmagnetic doping into host semiconductors can generate room-temperature ferromagnetism (RTF) of the whole solids.[9,10] In tackling the origin of such magnetism, it is apparently an urgent task to depict an unambiguous picture of the local electron density of states (LDOS) of the dopant, i.e., dopant states, particularly to position them in the electronic structures of the host semiconductors.[11,12] For Co-doped ZnO DMS nanostructures, one of the most studied prototypes of DMSs,[13−22] determining the Co dopant states and positioning them in the

† The University of Sydney.
‡ Soochow University.
§ Nanjing University.
|| Southeast University.
⊥ The Chinese University of Hong Kong.

(1) Erwin, S. C.; Zu, L.; Haftel, M. I.; Efros, A. L.; Kennedy, T. A.; Norris, D. J. *Nature* **2005**, *436*, 91–94.
(2) Bryan, J. D.; Gamelin, D. R. *Prog. Inorg. Chem.* **2005**, *54*, 47–126.
(3) Norris, D. J.; Efros, A. L.; Erwin, S. C. *Science* **2008**, *319*, 1776–1779.
(4) Nag, A.; Chakraborty, S.; Sarma, D. D. *J. Am. Chem. Soc.* **2008**, *130*, 10605–10611.
(5) Chen, D.; Viswanatha, R.; Ong, G. L.; Xie, R. G.; Balasubramaninan, M.; Peng, X. G. *J. Am. Chem. Soc.* **2009**, *131*, 9333–9339.
(6) Goodenough, J. B. *Magnetism and the Chemical Bond*; Interscience and John Wiley: New York, 1963.
(7) Wolf, S. A.; Awschalom, D. D.; Buhrman, R. A.; Daughton, J. M.; Von Molnar, S.; Roukes, M. L.; Chthelkanova, A. Y.; Treger, D. M. *Science* **2001**, *294*, 1488–1495.
(8) Coey, J. M. D.; Chambers, S. A. *MRS Bull.* **2008**, *33*, 1053–1058.
(9) Pan, H.; Yi, J. B.; Shen, L.; Wu, R. Q.; Yang, J. H.; Lin, J. Y.; Feng, Y. P.; Ding, J.; Van, L. H.; Yin, J. H. *Phys. Rev. Lett.* **2007**, *99*, 127201.
(10) Zhang, S. X.; Ogale, S. B.; Yu, W. Q.; Gao, X. Y.; Liu, T.; Ghosh, S.; Das, G. P.; Wee, A. T. S.; Greene, R. L.; Venkatesan, T. *Adv. Mater.* **2009**, *21*, 2282–2287.
(11) Sanvito, S.; Pemmaraju, C. D. *Phys. Rev. Lett.* **2009**, *102*, 159701.
(12) Walsh, A.; Da Silva, J. L. F.; Wei, S. H. *Phys. Rev. Lett.* **2008**, *100*, 256401.
(13) Schwartz, D. A.; Norberg, N. S.; Nguyen, Q. P.; Parker, J. M.; Gamelin, D. R. *J. Am. Chem. Soc.* **2003**, *125*, 13205–13218.

 10.1021/ja100912k

electronic structure of host ZnO are of first priority in understanding the origin of the RTF. However, it has still been equivocal in both theoretical and experimental aspects.[8]

Theoretically, density functional theoretical (DFT) calculations form a quantum chemistry solution to predict the magnetism based on the description of electronic structures of the DMSs, whereas critical debates lie at the correct positioning of dopant 3d levels and the Fermi level with respect to the host bands, as well as the incorporation degree of the dopant states.[11,12] The precise prediction of the LDOS positions is desired since the sensitive electron transportation of the dopant states can be dramatically tuned by the very minute shift of their positions, resulting in the contentious interpretations of the RTF of the DMSs.[11,12] However, directly reproducing the bandgap of semiconductors basically remains an unreliable task due to the consideration of additional particles in the calculations of empty bands.[23] The correct location of the dopant states even requires an artificial shift of the LDOS functions. It has to depend on experimental results as the external inputs, which at least requires a set of experimentally determined LDOS (e.g., LDOS of Zn, Co, and O in the present case).[12]

Experimentally, scaling the electron states from dilute dopants in the semiconducting nanostructures requires probes with both chemical (i.e., atomic specification) and spatial resolutions. However, it is generally a great challenge for the current optical spectroscopic techniques. For example, an extinction spectrum from visible optical absorption may be inverted to extract electronic structures, but the chemical resolution is hardly implemented due to the multiple excitation channels.[15] The extraction and quantification of a selected LDOS further suffer from the anomalous cross sections arising from the optical wave interference and transition resonances. Even for the valence-band photon-induced electron spectra and the deep ultraviolet spectra, which can provide ionization information on all the dopant states, the above-mentioned problem still exists and their quantification usually poses the problem of surface charge accumulation.[24]

Remarkably, core-loss electron energy-loss spectroscopy (EELS) attached in a scanning transmission electron microscope (STEM) has been well established with the chemical information on a subnanometer scale,[25,26] while valence EELS in the STEM possesses near-optical energy resolution and has been directly related to the LDOS of materials.[27] In this article, we employ these two techniques on the same nanorods by spatially mapping the dopant distribution via the core-loss electron energy-loss (EEL) spectra and simultaneously by identifying the dopant features in the accumulated valence EEL spectra via the measured dopant richness in the surface. Thus, the chemical resolution is implemented in the valence EELS technique besides its high spatial resolution. Here by taking Co-doped ZnO nanostructures as an example, the three Co dopant states related to the LDOS in individual ZnO nanostructures are successfully determined. The progress feeds the DFT calculations on the minimum input of the determined LDOS set. Thereby, a precise description of full electronic structures of Co-doped ZnO nanostructures is achieved for the first time. Local magnetic moments and related spin-coupling are then modeled, providing evidence for carrier-mediated RTF occurring in the Co-doped ZnO DMS system.

II. Methods

2.1. Synthesis and Characterization. The specimens of Co-doped ZnO nanostructures were synthesized by a simple solvothermal technique.[28] The Co concentration was determined to be ~7.85 at. % by induced coupled plasma atomic emission spectroscopy. The undoped ZnO sample was also prepared in the identical conditions for comparison. The Co-doped ZnO sample exhibits similar microstructures (see Figure S1 in the Supporting Information) and room-temperature ferromagnetic behavior to those previously reported.[22,28] The valence state of Co determined by X-ray photoelectron spectroscopy is divalent, and the saturation magnetic moment determined by the superconducting quantum interference device magnetometer is estimated to be $\sim 0.3\ \mu_B/Co^{2+}$, comparable with those of our previously synthesized samples.[28] The EELS measurements were performed in a STEM (VG HB 601UX) instrument. The microscope operated at 100 kV was equipped with a cold field-emission gun. The spatial resolution was estimated to be ~4 nm due to the delocalization effect of the electrons' inelastic scattering. Such resolution is adequate to identify the discrimination between the surface and the center of individual nanostructures with an average diameter of about 50 nm.[28] The energy resolutions were about 0.35 and 1.0 eV for the valence and core-loss EEL spectra, respectively, validating the investigations of the LDOS features within a few eV regions. A more detailed description of the valence EELS methodology can be found in the Supporting Information, S2.

2.2. Density Functional Theoretical Calculations. The electronic structures of $Zn_{11}O_{12}Co$ (Co concentration: ~8.3%) were determined using spin-polarized plane-wave DFT calculations, as implemented by the Vienna *Ab-initio* Simulation Package (VASP).[29] We adopted a projected augmented wave (PAW) pseudopotential[30] to describe the core electrons and the general gradient approximation (GGA) of Perdew, Burke, and Ernzerhof (PBE) for exchange and correlation.[31] The kinetic energy cutoff is 450 eV, and the Brillouin zone is sampled by $5 \times 5 \times 5$ *k*-points using the Monkhorst−Pack method.[32] To overcome the errors associated with the DFT self-interaction, a DFT + *U* method[33] was employed to calculate the on-site Coulomb correlation for the Zn and Co 3d electrons, and

(14) Coey, J. M. D.; Venkatesan, M.; Fitzgerald, C. B. *Nat. Mater.* **2005**, *4*, 173–179.
(15) Kittilstved, K. R.; Liu, W. K.; Gamelin, D. R. *Nat. Mater.* **2006**, *5*, 291–297.
(16) Liu, W. K.; Whitaker, K. M.; Kittilstved, K. R.; Gamelin, D. R. *J. Am. Chem. Soc.* **2006**, *128*, 3910–3911.
(17) Qiu, X. Q.; Li, L. P.; Tang, C. L.; Li, G. S. *J. Am. Chem. Soc.* **2007**, *129*, 11908–11909.
(18) Xu, Q. Y.; Hartmann, L.; Zhou, S. Q.; Mcklich, A.; Helm, M.; Biehne, G.; Hochmuth, H.; Lorenz, M.; Grundmann, M.; Schmidt, H. *Phys. Rev. Lett.* **2008**, *101*, 076601.
(19) Lu, Z.; Hsu, H. S.; Tzeng, Y.; Huang, J. C. A. *Appl. Phys. Lett.* **2009**, *94*, 152507.
(20) Liang, W.; Yuhas, B. D.; Yang, P. *Nano Lett.* **2009**, *9*, 892–896.
(21) Larde, R.; Talbot, E.; Vurpillot, F.; Pareige, P.; Schmerber, G.; Beaurepaire, E.; Dinia, A.; Pierron-Bohnes, V. *J. Appl. Phys.* **2009**, *105*, 126107.
(22) Zhang, Z. H.; Wang, X. F.; Xu, J. B.; Muller, S.; Ronning, C.; Li, Q. *Nat. Nanotechnol.* **2009**, *4*, 523–527.
(23) Badaeva, E.; Feng, Y.; Gamelin, D. R.; Li, X. *New J. Phys.* **2008**, *10*, 055013.
(24) Chiou, J. W.; et al. *Appl. Phys. Lett.* **2007**, *90*, 062103.
(25) Bosman, M.; Keast, V. J.; Garcia-Munoz, J. L.; D'Alfonso, A. J.; Findlay, S. D.; Allen, L. J. *Phys. Rev. Lett.* **2007**, *99*, 086102.
(26) Muller, D. A. *Nat. Mater.* **2009**, *8*, 263–270.
(27) Muller, D. A.; Singh, D. J.; Silcox, J. *Phys. Rev. B* **1998**, *57*, 8181–8202.
(28) Wang, X. F.; Xu, J. B.; Zhang, B.; Yu, H. G.; Wang, J.; Zhang, X. X.; Yu, J. G.; Li, Q. *Adv. Mater.* **2006**, *18*, 2476–2480.
(29) Kresse, G.; Furthmuller, J. *Phys. Rev. B* **1996**, *54*, 11169–11186.
(30) Kresse, G.; Joubert, D. *Phys. Rev. B* **1999**, *59*, 1758–1775.
(31) Perdew, J. P.; Burke, K.; Ernzerhof, M. *Phys. Rev. Lett.* **1996**, *77*, 3865–3868.
(32) Monkhorst, H. J.; Pack, J. D. *Phys. Rev. B* **1976**, *13*, 5188–5192.
(33) Anisimov, V. I.; Solovyev, I. V.; Korotin, M. A.; Czyzyk, M. T.; Sawatzky, G. A. *Phys. Rev. B* **1993**, *48*, 16929–16934.

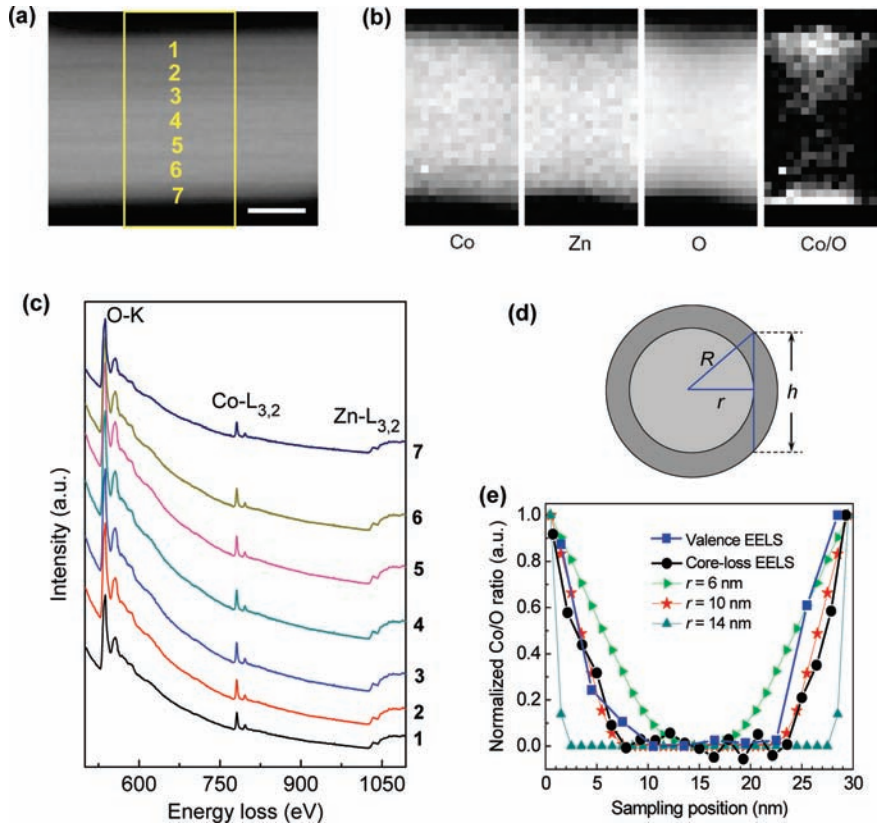

Figure 1. (a) HAADF image of the studied nanorod (diameter: ~30 nm). Scale bar, 10 nm. The boxed area shows the region where elemental maps and the core-loss EEL spectra are acquired. (b) Corresponding core-loss EEL maps of Co, Zn, and O elements at Co−L_3, Zn−L_3, and O−K edges, respectively. The intensities of the elemental maps are calculated by the procedure of peak fitting after the background is removed by a double-window method. The map of intensity ratios from Co/O is also included, where the darker intensities mean the smaller ratio of Co/O. (c) Core-loss EEL spectra acquired from 7 regions in the boxed area of the nanorod (a) with the corresponding numbers. The size of each region is about 20 × 4 nm^2. (d) Schematic cross-section illustration of the core−shell (radii are *r* and *R*, respectively) structure of the nanorod with the intensity ratio of Co/O in the shell decreasing linearly with the sampling position from the edge. (e) Finite-element calculation of the normalized intensity ratio of Co/O relative to the sampling position on the nanorod according to the model in (d). The experimental results of the normalized Co/O ratios acquired from the valence EEL spectra (blue curve) and core-loss EEL spectra (black curve) are also shown in (e) for comparison.

the states were corrected by $U - J = 1.5$ eV for Co and $U - J = 6.0$ eV for Zn.

III. Results and Discussion

3.1. Mapping Co Spatial Distribution by the Core-Loss EEL Spectra. We first map the Co concentration in selected individual Co-doped ZnO nanorods by core-loss EELS. This technique has been proved quite useful to investigate the nanoscale dopant distribution in a few kinds of DMS samples.[34−36] Figure 1a shows the high-angle annular dark field (HAADF) image of one nanorod, in which the yellow-boxed area is sampled for the concentration map. The intensities of the EEL spectra in the energy windows of Co−L_3, Zn−L_3, and O−K edges are calculated for each sampling point, which forms a pixel in the EEL maps of Co, Zn, and O elements, respectively (Figure 1b). Their intensities are obtained by the multipeak Gaussian fitting of the Co−L_3, Zn−L_3, and O−K edges. We further divide the Co intensity by that of O and obtain the Co/O map (Figure 1b). Note that the intensity ratios of L_3/L_2 white line peaks have long been regarded as a quantitative probe of dopant concentrations, and so are the Zn and O features.[37−39] Therefore, the bright edge in the Co/O map reveals the Co richness along the edge of the studied nanorod. A similar profile is also obtained for the Co/Zn ratio.

Furthermore, we collected the core-loss EEL spectra along the transverse direction and acquired a series of spectra with different positions across the nanorod (Figure 1c). The normalized intensity ratio of Co−L_3/O−K is calculated, yielding the Co/O profile of the black curve as shown in Figure 1e. These spectra with adequate spectroscopic counts further confirm the Co richness along the edge of the nanorod. We calculate several probable EEL Co/O profiles (Figure 1e) using a finite-element calculation based on the core−shell model (Figure 1d), where the measured values of the beam intensities are used for the different depths. The nanorod with a 5 nm Co-rich shell (i.e., $r = 10$ nm) fits the experimental results very well, as deduced from Figure 1e. Such an observation of a heavily doped shell surrounding an underdoped core is in good agreement with

(34) Ogale, S. B.; Choudhary, R. J.; Buban, J. P.; Lofland, S. E.; Shinde, S. R.; Kale, S. N.; Kulkarni, V. N.; Higgins, J.; Lanci, C.; Simpson, J. R.; Browning, N. D.; Das Sarma, S.; Drew, H. D.; Greene, R. L.; Venkatesan, T. *Phys. Rev. Lett.* **2003**, *91*, 077205.
(35) Chen, J. J.; Yu, M. H.; Zhou, W. L.; Sun, K.; Wang, L. M. *Appl. Phys. Lett.* **2005**, *87*, 173119.
(36) Ogale, S.; Kundaliya, D.; Mehraeen, S.; Fu, L. F.; Zhang, S. X.; Lussier, A.; Dvorak, J.; Browning, N.; Idzerda, Y.; Venkatesan, T. *Chem. Mater.* **2008**, *20*, 1344–1352.
(37) Pearson, D. H.; Ahn, C. C.; Fultz, B. *Phys. Rev. B* **1993**, *47*, 8471–8478.
(38) Ding, Y.; Wang, Z. L. *J. Electron Microsc.* **2005**, *54*, 287–291.
(39) Leapman, R. D.; Grunes, L. A. *Phys. Rev. Lett.* **1980**, *45*, 397–401.

previous observations in the single P-doped Ge nanowire[40] and B-doped Si nanowires,[41] indicating that our technique sufficiently discriminates the dopant spatial distribution. The measurements of the core-loss EELS on other individual nanorods further consolidate such an inhomogeneity. Note that it does not induce any secondary phase segregation in Co-doped ZnO nanostructures.[22,28]

3.2. Positioning Co Dopant States by the Accumulated Valence EEL Spectra. Obtaining the dopant inhomogeneous distribution, we now carry out the valence EELS measurements on the nanostructures and search for the coincidentally growing valence EEL features. Note that the valence EEL spectra before 5 eV are cut due to the possible mixing with the electron excitation from dopant states to the conduction band of ZnO (the interband transitions). In most cases, the dopant states of interests are located within a few eV from the Fermi level in the electronic structure of the host solid. It can exclude the presence of features excited from the dopant states to the empty conduction band after 5 eV in the valence EEL spectra. Such an argument is further verified by the DFT calculations (see below), which guarantee that the obtained features are attributed to the excitation from Co dopant states to vacuum (or near-vacuum) level. Thus, the underlying LDOS information can be extracted. In order to extract the dopant features successfully, it should be noted that the dopant signals are initially quite weak as compared to the primary featured groups such as plasmonic oscillation and interband (or intraband) transitions due to the quite distinct excitation probabilities (see the raw valence EEL spectra in Figures S2 and S3 in the Supporting Information).[38] The valence EEL spectra are obtained through accumulations of more than 5000 times the initial spectrum until the features with adequate signal-to-noise ratios are attained (for more details see the Supporting Information, S3 and S4).[42,43] In this way, the Co dopant states are successfully identified.

The 3d electrons of the Co dopant were previously reported to exert three main features in the host ZnO bands.[12,15,44] They are located (from vacuum energy) near the bottom of the conduction band (~6−7 eV), in the deep forbidden band (~9 eV), and in the valence band (~11 eV), respectively (Figure 2a). They have been attributed to the mainly minority-spin Co t_2 state, a minority-spin Co e state, and a majority-spin Co state containing both t_2 and e symmetries, respectively.[12,44] Their corresponding spectroscopic features are found and labeled by Co dopant state (i) (Co DS (i)), Co DS (ii), and Co DS (iii), as seen in the valence EEL spectra (Figure 2b,c). Deconvolution by the Richardson−Lucy algorithm[42,43,45] has been carried out to restore the Co DS (i) feature at ~6.2 eV in the valence EEL spectra (Figure 2b,c). The observation confirms the tetrahedral crystal field surrounding the Co ions in the ideal substituent sites of individual ZnO nanostructures.[12,15,22] Note that the Co DS (ii) feature is combined with the intense peak centered at

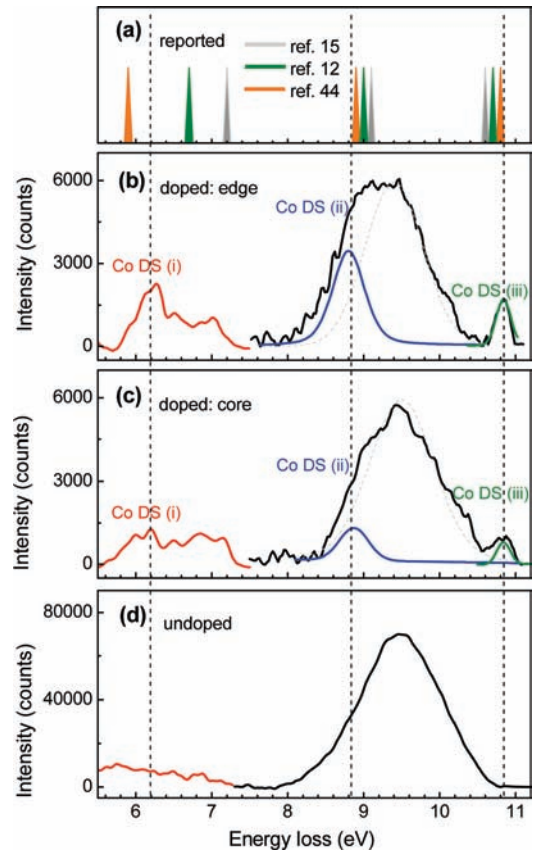

Figure 2. (a) Reported locations of the three Co 3d states of Co-doped ZnO, adopted from refs 12, 15, and 44, respectively. (b−d) Valence EEL spectra acquired from the edge region of the Co-doped ZnO nanorod (b), the core region of the same Co-doped ZnO nanorod (c), and the undoped ZnO nanorod (d). Peaks are fitted to explicitly show the features named by Co DS (ii), which is adjacent to the intense peak from the O 2p state of the host ZnO. The Richardson−Lucy algorithm is applied for Co DS (i) with the restored features as shown in the figure. The dashed lines are drawn as guides for the eyes.

~9.5 eV, which is ascribed to O 2p interband transition of the host ZnO.[38,46]

Correlation of the featured intensities with the Co concentration as well as the validity of the LDOS quantification is shown by the coincidence of valence EEL spectra with the corresponding core-loss EELS measurements (Figure 1e). The three well-defined features do emerge after the doping, and their intensities increase with increasing Co concentration (Figure 2b,c,d). We accumulate the valence EEL spectra along the edge (Figure 2b) and in the center (Figure 2c) of the individual nanorod with a diameter of ~30 nm, from which one can find the three Co features are more pronounced along the edge as compared to that in the center of the nanorod. A line profile of the normalized intensity ratio of Co DS (ii)/O 2p state is plotted by the blue curve in Figure 1e. It can be seen that the trends of these two line profiles (from valence EEL spectra and core-loss EEL spectra, respectively) are quite similar, verifying that the dopant features (Figure 2b,c) originate from Co dopant states and they contain the coincidental information for quantification. In addition, our DFT calculations reproduce the positions of the three Co-related peaks (Figure 3a,b). Therefore, the above evidence consolidates both the existence and positions of the three Co dopant states in the host ZnO bands.

(40) Perea, D. E.; Hemesath, E. R.; Schwalbach, E. J.; Lensch-Falk, J. L.; Voorhees, P. W.; Lauhon, L. J. *Nat. Nanotechnol.* **2009**, *4*, 315–319.
(41) Garnett, E. C.; Tseng, Y. C.; Khanal, D. R.; Wu, J.; Bokor, J.; Yang, P. *Nat. Nanotechnol.* **2009**, *4*, 311–314.
(42) Nelayah, J.; Kociak, M.; Stéphan, O.; García de Abajo, F. J.; Tencé, M.; Henrard, L.; Taverna, D.; Pastoriza-Santos, I.; Liz-Marzán, L. M.; Colliex, C. *Nat. Phys.* **2007**, *3*, 348–353.
(43) Song, F. Q.; Wang, T. Y.; Wang, X. F.; Xu, C. H.; He, L. B.; Wan, J. G.; Van Haesendonck, C.; Ringer, S. P.; Han, M.; Liu, Z. W.; Wang, G. H. *Small* **2010**, *6*, 446–451.
(44) Pemmaraju, C. D.; Hanafin, R.; Archer, T.; Braun, H. B.; Sanvito, S. *Phys. Rev. B* **2008**, *78*, 054428.
(45) Gloter, A.; Douiri, A.; Tence, M.; Colliex, C. *Ultramicroscopy* **2003**, *96*, 385–400.
(46) Wang, J.; Li, Q.; Egerton, R. F. *Micron* **2007**, *38*, 346–353.

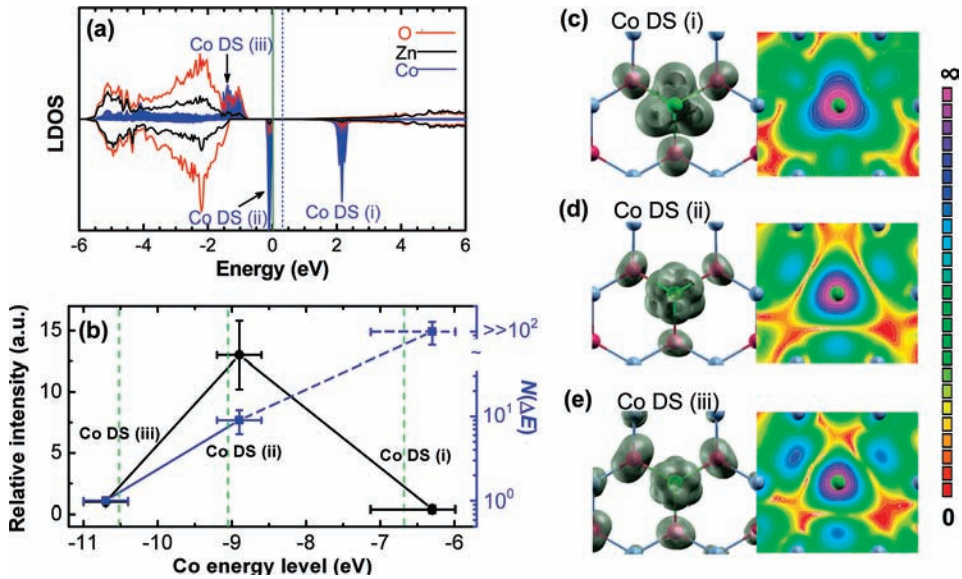

Figure 3. (a) Calculated LDOS for the $Zn_{11}O_{12}Co$ supercell by the DFT + U method. The LDOS of Co is shaded in blue. The vertical green line indicates the Fermi level, and the blue dashed line indicates the conduction band minimum from a pure ZnO supercell. The areas of the three Co features of Co DS (i), Co DS (ii), and Co DS (iii) are 42.0, 32.9, and 24.7 states, respectively. (b) Experimental peak intensities (left axis) and estimated $N(\Delta E)$ (right axis) of the three dopant states against their energies. The calculated locations (marked by the dashed green lines) of the three Co 3d states are also shown here, which agree well with the experimental locations within the errors. The range of Co DS (i) position is broad and asymmetric due to the low signal/noise ratio and the applied Richardson-Lucy deconvolution. $N(\Delta E)$ of Co DS (i) is deduced by its position at the onset of the conduction band; therefore it is marked by the dashed line. All the solid/dashed lines are drawn as guides for the eyes. (c−e) Spatial distribution of the charge density isosurface for the three features labeled by Co DS (i), Co DS (ii), and Co DS (iii), respectively. One can see the increasing extension of charges around the Co ion from Co DS (iii) to Co DS (i), which is in accordance with the experimental observations.

3.3. Corrected Full Electronic Structures by the DFT Calculations and Quantitative Analysis of Co Dopant States. The DFT + U method for first-principles calculations is carried out with the experimental inputs of the positions of the dopant states, which results in the full electronic structures of the Co-doped ZnO (including the LDOS of O and Zn), as shown in Figure 3a. Note that only the input of relative positions of Co dopant states can optimize the corrected full electronic structures. In Figure 3a, all the inputs are well reproduced. The bandgap of ~3.0 eV is obtained. Co DS (i) is located at the onset of the conduction band, Co DS (ii) is within the bandgap, and Co DS (iii) is located in the valence band. The Fermi level is located near Co DS (ii). It can be seen that the LDOS of Co is hybridized with that of O.

The obtained density of the electron states helps the quantitative analysis of the dopant states and the associated bulk performance. As known, the appearance of the interesting intrinsic RTF observed in Co-doped ZnO[22,28] has to do with both the generation of local magnetic moments and the effective coupling between the magnetic sites.[47] The magnetic dopant states should be transported in a long range to construct the effective ferromagnetic coupling,[6] so that they are able to manipulate the macroscopic RTF occurring in Co-doped ZnO. This picture is essentially related to the incorporation strength of the dopant states, i.e., their extension in the entire host solid. Here the term "extension" means the chance of observing the electrons or charges of the state at the sites far from the dopant ions rather than that of hybridization. Here, the electron extension degree can be semiquantitatively assessed by analyzing the intensities of the dopant features based on the picture including the single-particle scattering and the multiple-atom effect (for more details see the Supporting Information, S5).[37,48]

In a typical EEL procedure that occurs with the three dopant features, the incident high-energy electrons (100 keV) knock the electrons in the initial level (the dopant states) up to an empty vacuum (or near-vacuum) level. The present configuration of the electron beam and the collection detectors leads to the single-particle scattering of collected electrons, validating the quantification of the incident electrons (including the thermal diffuse scattering).[37,49] In the case of the unoccupied final states, the transition matrix turns to the occupied LDOS of the initial levels.[27] Therefore, the EEL intensity of a selected state is closely related to the quantity of its present electrons. However, the description that the electrons' interaction with the incident fast electrons stays localized within an individual atom becomes questionable for Co 3d electrons that are spatially located near (or even over) the edge of Co ions. The collective contribution from neighboring atoms to the dopant features (Figure 2b,c) leads to the intensity increase, i.e., the multiple-atom effect. Here the ratio of the experimentally collected electrons as compared to the single-atom description is denoted as $N(\Delta E)$, which describes the strength of multiple-atom effects in the electron scattering. It has the dimension of the atom quantity that contributes to the scattering of a selected electron. As a result, $N(\Delta E)$ becomes the index of electron extension degree of the Co 3d states in the host ZnO.

According to the Fermi−Dirac distribution at the present liquid nitrogen temperature (down to 77 K), the occupation of Co DS (ii) and Co DS (iii) should both be close to 100% since they are located below the Fermi level. Hence, $N(\Delta E)$ can be

(47) Dev, P.; Xue, Y.; Zhang, P. H. *Phys. Rev. Lett.* **2008**, *100*, 117204.
(48) Pearson, D. H. Ph.D. thesis, California Institute of Technology, CA, 1992.
(49) Howie, A. *J. Microsc.* **1979**, *117*, 11–23.

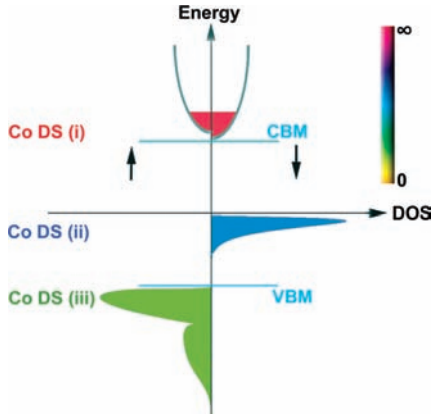

Figure 4. Schematic energy diagram, indicating the construction of room-temperature magnetism. The three dopant states are positioned according to the experimental measurements. The Co DS (ii) and Co DS (iii) are below the Fermi level; the Co DS (i) is partially occupied by few electrons, which promises a stable state with a net robust ferromagnetism according to the band-coupling model. The locations of conduction band minimum (CBM) and valence band maximum (VBM) are also shown in the energy diagram. The electron extension degree is marked by the color depth bar.

semiquantitatively estimated by comparing the measured intensities and the calculated LDOS intensities, which gives a larger $N(\Delta E)$ for Co DS (ii) than that for Co DS (iii). Co DS (i) is located at the onset of the conduction band, and its extension degree must be quite intense. Therefore, with increasing state energies, we obtain a gradual transition from the relatively localized state (Co DS (iii)) to a rather extended one (Co DS (i)) (Figure 3b). Such an argument is further verified by the calculated maps of charge density isosurface (Figure 3c−e), where we can clearly see the gradually increasing extension of charges around the Co ion from Co DS (iii) to Co DS (i). Our observation is consistent with Mott's prediction that the electron extension degree increases with the radius of the electron state.[50]

3.4. Explanation of Carrier-Mediated RTF. The measured electronic structures from core-loss and valence EEL spectra and the extension degrees of the dopant states can build the intrinsic magnetism against room temperature in the framework of carrier-mediated RTF (as summarized in Figure 4).[12] The DFT calculations of a $Zn_{11}CoO_{12}$ supercell attain a spin-dependent LDOS curve and give a local magnetic moment of 2.9 μ_B per Co ion (Figure 3a). The calculations demonstrate a ferromagnetic state in which fully occupied Co DS (iii) is spin-up, while Co DS (i) and Co DS (ii) are spin-down. The calculations indicate that most of the charges are still localized in the above three dopant states. Therefore, a local high-spin state is constructed, which is the first point of the RTF interpretation. The second point lies at whether such a ferromagnetic state is able to survive the perturbation of ambient conditions.[47] It has to be implemented through the effective coupling of neighboring spin states. The recent calculations based on the crystal-field theory concluded an antiferromagnetic coupling in the case of no free carrier or no defect states.[12,44] Herein we successfully detect the Co DS (i) state in the conduction band, which demonstrates an observable carrier density on the order of less than 0.1 electron per Co ion. Although it introduces certain inverse spins, it stabilizes the ferromagnetic coupling against the ambient conditions according to the band-coupling model,[12] ultimately leading to the RTF. The third point is that we have observed the saturation magnetic moments of less than 1.0 μ_B per Co ion. Such a moderate value is attributed to the state-dependent electron extension degree. The Heisenberg model addresses the exchange energy as the origin of ferromagnetic coupling, which is related to the overlapping of the energy states between neighboring units. The measured electron extension degree or the multiple-atom effect essentially describes such an overlapping. The spin-down states of Co DS (ii) and Co DS (i) present the higher electron extension degrees. Such a significantly enhanced extension degree for Co DS (i) leads to a greater exchange energy and a more effective coupling of the spin-down states. Overall, the evidence demonstrates a carrier-mediated picture (Figure 4) on the moderate RTF occurring in Co-doped ZnO nanostructures, which is consistent with a recent report.[12]

IV. Conclusions

In summary, chemical identification has been implemented in the valence EELS technique by tracking the coincidentally growing dopant features in individual ZnO nanostructures as demonstrated by the core-loss EELS mapping. We have obtained an overall description of the three Co dopant states and their extension degrees in the host ZnO bands, which is further reproduced by the first-principles calculations. From these results, we finally depict a carrier-mediated picture on the interpretation of the moderate intrinsic RTF occurring in Co-doped ZnO nanostructures. We believe that the chemically resolved EELS tool to determine the electronic structures on a nanometer scale may find applications in other doped functional systems.

Acknowledgment. We thank Prof. S.-H. Wei and Dr. A. Walsh (National Renewable Energy Laboratory, USA), Prof. S. A. Chambers (Pacific Northwest National Laboratory, USA), Prof. S. Sanvito and Dr. C. D. Pemmaraju (Trinity College, Ireland), Prof. Q. Li (The Chinese University of Hong Kong, China), Prof. S. P. Ringer (The University of Sydney, Australia), and Prof. C.-D. Gong (Nanjing University, China) for valuable and stimulating discussions and S. Bulcock and Dr. R. K. Zheng for technical assistance. This work was supported by grants from the National Natural Science Foundation of China (10904100, 10674056, 20873019, and 90606002), the National Key Projects for Basic Research of China (2010CB923401 and 2009CB930501), the Start-up Funding through 211 Project at Soochow University of China (14108001), the Australian Research Council (DP0770987), and the Research Grants Council of Hong Kong SAR (N_CUHK447/07). We acknowledge the AMMRF facilities for the use of instrumentation.

Supporting Information Available: TEM image (Figure S1), more detailed description of the valence EELS methodology and valence EEL data processing and errors (Figure S2), raw valence EEL spectra (Figure S3), additional notes on understanding intensities of the valence EEL spectra quantitatively, and complete ref 24. This material is available free of charge via the Internet at http://pubs.acs.org.

JA100912K

(50) Mott, N. F. *Nuovo Cimento* **1958**, *7* (Suppl.), 312–328.